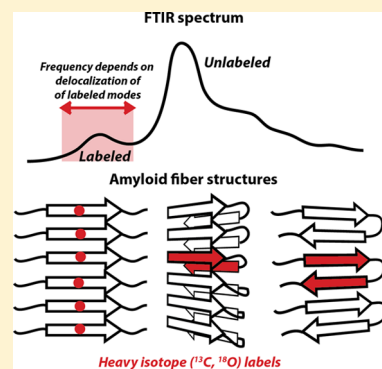


## How to Get Insight into Amyloid Structure and Formation from Infrared Spectroscopy

Sean D. Moran and Martin T. Zanni\*

Department of Chemistry, University of Wisconsin—Madison, 1101 University Avenue, Madison, Wisconsin 53706, United States

**ABSTRACT:** There is an enormous amount of interest in the structures and formation mechanisms of amyloid fibers. In this Perspective, we review the most common structural motifs of amyloid fibers and discuss how infrared spectroscopy and isotope labeling can be used to identify their structures and aggregation kinetics. We present three specific strategies, site-specific labeling to obtain residue-by-residue structural information, isotope dilution of uniformly labeled proteins for identifying structural folds and protein mixtures, and expressed protein ligation for studying the domain structures of large proteins. For each of these methods, vibrational couplings are the source of the identifying features in the infrared spectrum. Examples are provided using the proteins hIAPP, A $\beta$ , polyglutamine, and  $\gamma$ D-crystallin. We focus on FTIR spectroscopy but also describe new observables made possible by 2D IR spectroscopy.



The amyloid state of proteins and peptides is characterized by the formation of ordered aggregates with fibrous morphology.<sup>1,2</sup> First identified over 150 years ago, amyloid deposits in tissue have since been linked to over 20 human diseases, and over 40 different proteins have been identified in potentially pathogenic aggregates. Diseases such as Alzheimer's disease, Parkinson's disease, prion diseases, and type II diabetes have all been linked to amyloid aggregates or toxic intermediates in their formation.<sup>2</sup> More recently, the role of amyloid aggregates in biology has been shown to include functional amyloids that are required for specific biological functions such as the formation of melanin and bacterial biofilms.<sup>3</sup> These functional amyloids have inspired the use of fibrous amyloid species as components of synthetic nanoscale materials,<sup>4–6</sup> with possible applications in nanoscale electronics, nonlinear optics, and as structural components of composite materials. Moreover, it has become clear that the ability to form amyloid aggregates is not limited to disease-related proteins and natural functional amyloids; in fact, a majority of proteins contain sequences with high amyloid fibrillation propensity,<sup>7</sup> and it has been suggested that the amyloid state may represent the global free-energy minimum of most proteins.<sup>8</sup> Thus, a detailed understanding of amyloid protein structures and the mechanisms through which they form is not only important in the biochemistry of disease and in materials science but would also answer fundamental questions regarding the nature of protein folding. The accompanying Guest Commentary by Raleigh provides an excellent overview of the amyloid field, and the two companion Perspectives by Shea and Ramamoorthy provide insights into one of the most prevalent and well-studied amyloid-forming proteins, human islet amyloid polypeptide (hIAPP or amylin). Our research group also studies hIAPP. In this Perspective, we focus on new approaches to probing the structures and formation mechanisms of amyloid aggregates using infrared spectroscopy and isotope labeling that we have

applied to hIAPP and other amyloid-forming proteins including polyglutamine (polyQ) and  $\gamma$ D-crystallin.

IR spectroscopy has provided insights into amyloid aggregation not easily obtained by other methods.

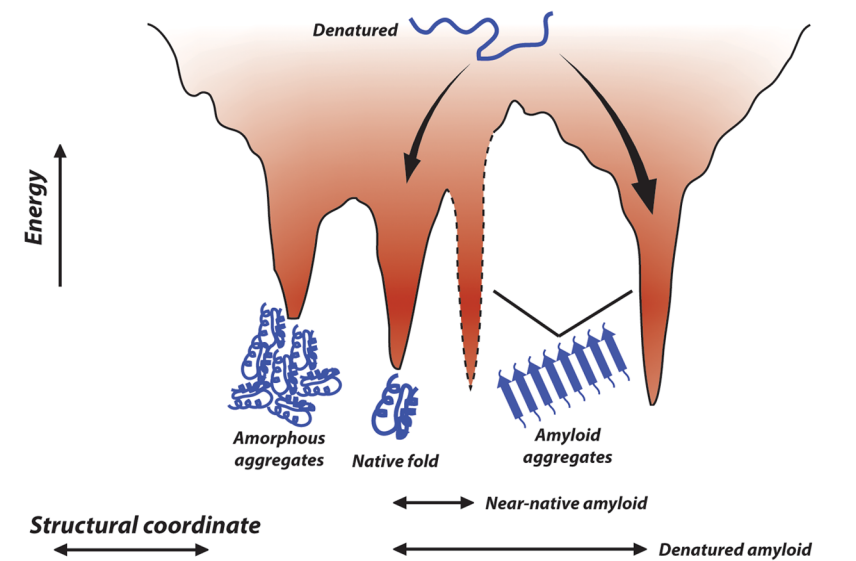
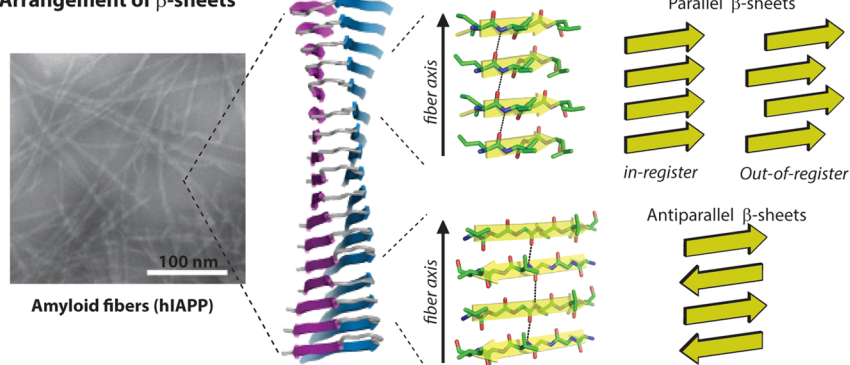
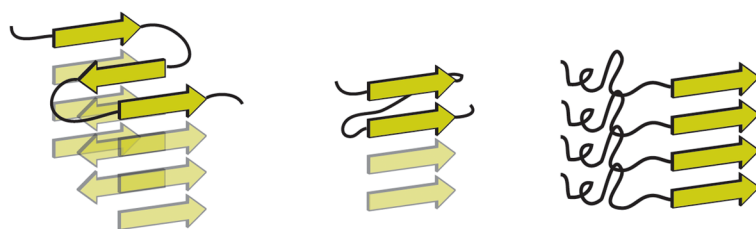
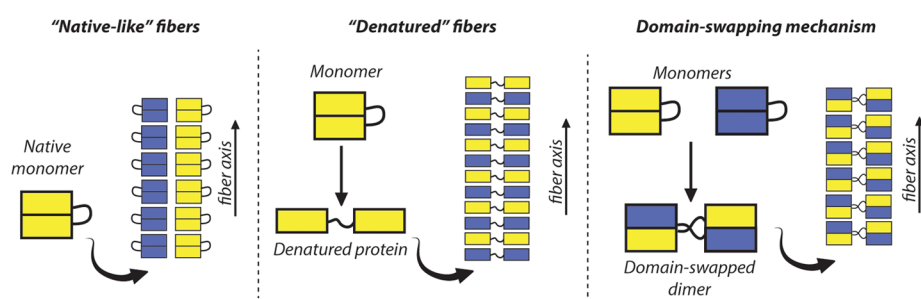
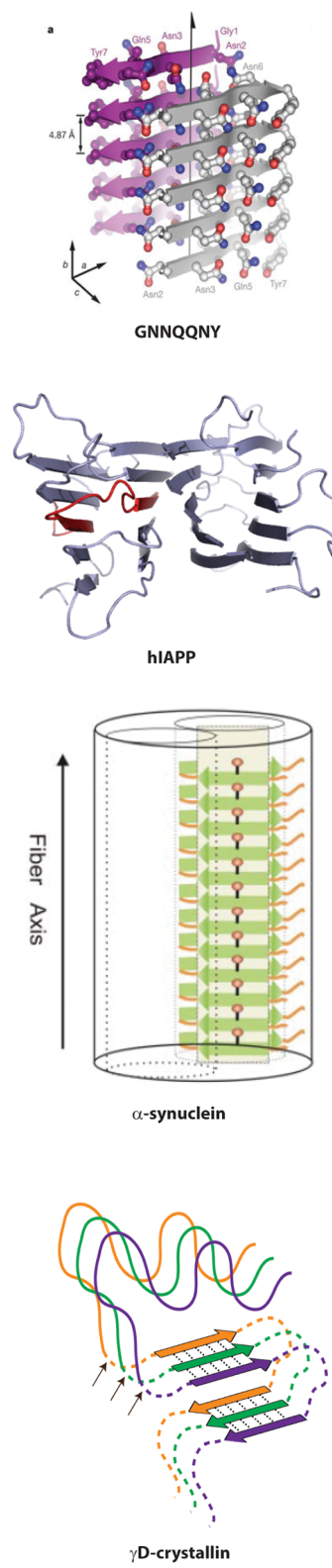
The main structural features of amyloid aggregates are extended, intermolecular  $\beta$ -sheets with  $\beta$ -strands oriented perpendicular to the fiber axis, in what is known as a cross- $\beta$  architecture.<sup>2,9</sup> Historically, the amyloid state of proteins has been assigned based on a number of experimental criteria including fibrous morphology in electron micrographs, specific dye-binding activity, and fiber X-ray diffraction patterns consistent with the extended  $\beta$ -sheets of their cross- $\beta$  structures.<sup>9</sup> Other methods, including atomic force microscopy, infrared absorption, and Raman spectroscopy, have also been used to identify the amyloid nature of individual aggregate species.<sup>10</sup> More detailed structural information comes from X-ray crystallography of amyloid fragments and solid-state NMR spectroscopy of fragments and polypeptides.<sup>2,11–17</sup> Together, these techniques have uncovered a wide structural diversity of the amyloid state and basic principles for the stabilizing factors of amyloid formation, which serve as guides for understanding larger and more complex amyloid systems.

Figure 1 summarizes typical amyloid fiber structures and formation mechanisms compiled from recent examples in the chemical literature. These examples demonstrate the diversity

Received: April 21, 2014

Accepted: May 16, 2014

Published: May 16, 2014

**A. Protein misfolding and aggregation****B. Arrangement of  $\beta$ -sheets****C. Supramolecular  $\beta$ -sheet architectures****D. Aggregation and fiber models****E. Examples**

**Figure 1.** Structures of amyloid fibers. (A) Schematic of a protein folding free-energy landscape. Amyloid aggregates occupy a low-energy well in this landscape that can contain structural configurations very different from those of the native state and native-like amorphous aggregates. Adapted from Hartl et al., ref 24, copyright 2011, Nature Publishing Group. (B) Arrangement of  $\beta$ -sheets. Amyloid fibers (left, from ref 25, copyright 2012, Nature Publishing Group) are composed of one or more protofibrils (center) containing stacks of  $\beta$ -strands running perpendicular to the protofibril axis ("cross- $\beta$ " structure).<sup>26</sup> The protofibril model is reproduced from ref 26, copyright 2010, FASEB. Cross- $\beta$  structures may contain either parallel (right, top) or antiparallel (right, bottom)  $\beta$ -strands that may be either in-register or out-of-register. (C) Supramolecular  $\beta$ -sheet architectures. Each

Figure 1. continued

protein can contribute  $\beta$ -strands to multiple  $\beta$ -sheets (left) or multiple  $\beta$ -strands to each  $\beta$ -sheet (center). Non- $\beta$  conformations may also exist outside of the stable fiber core (right). (D) Aggregation and fiber models. A number of aggregation models relevant to amyloid formation have been proposed, including direct incorporation of native monomers into the aggregates (left), the incorporation of denatured monomers or oligomers into the aggregates (center), or the formation of domain-swapped dimers or oligomers that form fibers (right) as in cystatin C.<sup>27</sup> (E) Examples of structural models of amyloids from prior publications (top to bottom): yeast prion fragment GNNQQNY via X-ray crystallography;<sup>11</sup> hIAPP via ssNMR spectroscopy (coordinate file provided by R. Tycko);  $\alpha$ -synuclein via site-directed spin labeling and EPR;<sup>18</sup> and  $\gamma$ D-crystallin via 2D IR spectroscopy.<sup>19</sup> The structural model of GNNQQNY is reprinted by permission from Macmillan Publishers Ltd.: Nature (ref 11), copyright 2005. The structural model of  $\alpha$ -synuclein was reproduced from ref 18. This research was originally published in The Journal of Biological Chemistry, copyright 2007, the American Society for Biochemistry and Molecular Biology.

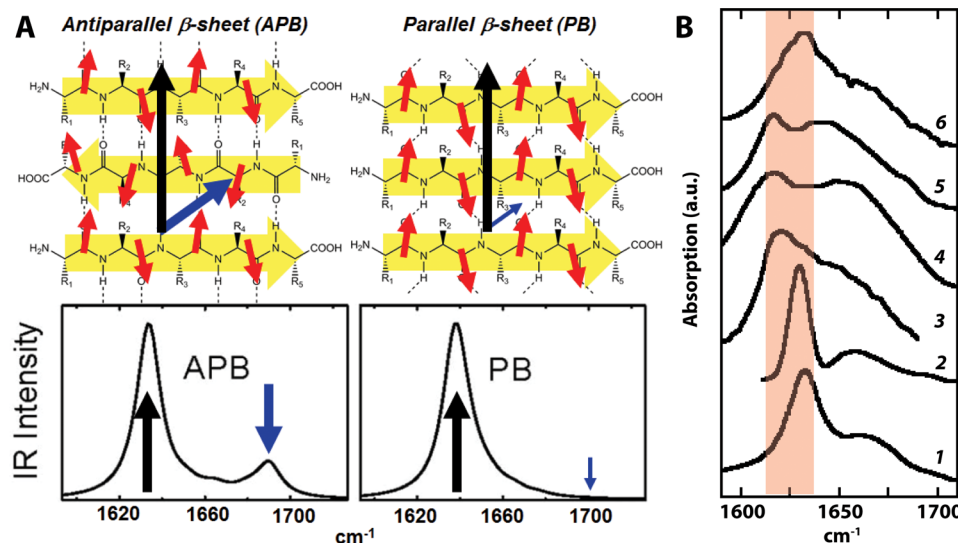


**Figure 2.** Amide I modes of (amyloid)  $\beta$ -sheets. (A) Amide I vibrational modes in  $\beta$ -sheets.  $\beta$ -sheets may form in either parallel or antiparallel orientations. In each, extensive hydrogen-bonding arrays between peptide bonds in neighboring strands stabilize the structure. The transition dipole moments of these peptide bonds can be represented in either a local or normal mode basis. Local modes (red arrows) are oriented approximately along the C=O bonds and are of similar magnitude for each residue. Vibrational coupling between these transition dipole moments leads to excitonic delocalization within the  $\beta$ -sheet, corresponding to the normal modes of the system (black, blue arrows). In the IR spectra of  $\beta$ -sheets, two such modes are prominent, one in which vibrations are delocalized between strands or along an amyloid fiber axis and one that lies approximately parallel to the strands. Antiparallel and parallel  $\beta$ -sheets differ primarily in the strength and frequency of the latter mode, while the former is strong in both kinds of systems. Lower panels are reprinted, with permission, from ref 33, copyright 2005, AIP Publishing LLC. (B) FTIR spectra of amyloid fibers show the presence of a strong absorbance in the region of 1615–1630  $\text{cm}^{-1}$ , corresponding to the highly delocalized modes oriented along the fiber axis (red shaded region). Data are taken from (1)  $\beta$ 2-microglobulin<sub>21–31</sub>,<sup>39</sup> (2)  $\text{A}\beta$ ,<sup>40</sup> (3) hIAPP,<sup>41</sup> (4) PrP,<sup>42</sup> (5)  $\gamma$ D-crystallin,<sup>43</sup> and (6)  $\alpha$ -synuclein.<sup>44</sup>

of proposed amyloid structures and the challenges inherent in their characterization. The primary goal of this Perspective is to explain methods and provide examples for which infrared spectroscopy and isotope labeling can uncover motifs like these.

The cross- $\beta$  arrangement of amyloid fibers comes from repeated arrays of intermolecular hydrogen-bonded  $\beta$ -strands from multiple protein or peptide molecules. This cross- $\beta$  structure, in which  $\beta$ -strands are arranged approximately perpendicular to the fiber axis, results in the familiar protofibril structure (Figure 1B), which is the basic unit of an amyloid fiber. One or more protofibrils may associate to form the mature fiber structure. Within each protofibril,  $\beta$ -strands may be arranged in either an antiparallel or parallel orientation. The  $\beta$ -sheets can be further divided into either “in-register” sheets with identical sequence positions aligned with one another or “out-of-register” sheets in which identical positions do not interact directly via hydrogen bonds. Each of these  $\beta$ -sheet variants has been characterized in detail in crystallographic studies of short sequence fragments of amyloid polypeptides,<sup>2,11,13,14</sup> providing important insight into the stabilizing forces of these cross- $\beta$  structures. In larger amyloid proteins,

including natural sequences of over 100 amino acids such as  $\alpha$ -synuclein,<sup>18</sup>  $\gamma$ D-crystallin,<sup>19</sup> tau, and others, the conformations of individual protein molecules in the fiber state must be much more complex<sup>15</sup> because  $\beta$ -strands with more than 15 amino acids are rare.<sup>20</sup> In such cases, multiple  $\beta$ -strands per protein are likely, with each protein contributing strands to multiple  $\beta$ -sheets or multiple strands to each  $\beta$ -sheet with a mixture of intramolecular and intermolecular hydrogen bonds (Figure 1C). Additionally, large segments of sequence may exist outside of the cross- $\beta$  core of amyloid fibers, adopting non- $\beta$  structures including helices, turns, or disordered conformations.<sup>19,21</sup>

The probability of any given sequence forming amyloid aggregates depends on the accessibility of the amyloid state within the protein’s folding free-energy landscape,<sup>7</sup> in particular, the number and height of barriers between the native state and the amyloid state. On the basis of structural models of amyloid aggregates, some amyloid species, such as domain-swapped aggregates including cystatin c,<sup>22</sup> have molecular conformations very similar to those of their native states, while the misfolded states of others bear little resemblance to their known native structures (Figure

1D).<sup>19,23</sup> A comparison of a protein's native and amyloid conformations provides insight into the structural perturbations that must occur to access the misfolded state but does not reveal the mechanism of amyloid aggregation, which may contain numerous intermediate states.<sup>28</sup> Structural information describing these transient states is necessary for a complete understanding of the amyloid aggregation processes, but to date, few intermediate structures have been characterized.<sup>28</sup> Finally, Figure 1E illustrates some published models for higher-order structures of fibers.

Given the diversity and complexity of proposed amyloid structures (Figure 1E), the importance of transient intermediates in their aggregation mechanisms, and the likely dependence of misfolded structures on aggregation conditions, experimental techniques capable of addressing both stable molecular structures and aggregation kinetics under a variety of conditions are needed. Infrared spectroscopy has a number of features that make it particularly well-suited to the analysis of amyloid structure and mechanism. First, IR frequencies and line shapes in the amide I region of a protein IR spectrum are sensitive to protein secondary structure. Second, IR spectra can be collected on a broad range of samples, including heterogeneous suspensions of aggregated proteins and membrane-bound amyloids. Third, the sample requirements for IR spectroscopy are small (microgram scale),<sup>19</sup> so that even difficult proteins can be analyzed under a variety of different conditions. Finally, data acquisition is rapid, enabling the determination of structural information in kinetics experiments.<sup>29</sup> The major drawback of infrared spectroscopy is spectral congestion; one can identify that a  $\beta$ -sheet is present, for example, but not which amino acids contribute to that  $\beta$ -sheet. However, this drawback can be mitigated with an understanding of vibrational couplings and the use of isotope labels. On the basis of this understanding, IR spectroscopy has provided insights into amyloid aggregation not easily obtained by other methods.

*Origin of Characteristic Amyloid Features in Infrared Spectra.* Infrared spectroscopy, namely, FTIR spectroscopy, is often used to diagnose amyloid formation because the amide I regions of amyloid fibers are dominated by a narrow, intense absorption that falls between 1615 and 1630  $\text{cm}^{-1}$ .<sup>30–33</sup> This frequency range is lower than that of typical  $\beta$ -sheets ( $>1630 \text{ cm}^{-1}$ ) because the  $\beta$ -sheets of amyloids are usually large and extremely well-ordered, which results in vibrational motions that extend along large sections of the fiber backbone. This phenomenon can be understood and used to probe structures by visualizing the arrangement of the amide I vibrations from each individual amino acid, which are called "local modes" in the jargon of spectroscopists. The amide I vibrational mode is mostly C=O with a little C–N stretch (Figure 2A, red arrows), giving rise to a vibrational transition dipole that dictates the magnitude and direction that infrared radiation would most likely be absorbed if it were a single, isolated amino acid. In a polypeptide or protein, the amino acids are not isolated. Instead, they are close enough that their transition dipoles become coupled to one another. As a result, each amino acid no longer vibrates individually, but they vibrate in unison in motions that are called "normal modes". Because they involve more than one transition dipole, normal mode vibrations are extended across multiple amino acids. They are typically larger, point in different directions, and absorb at a different frequency than the local mode transition dipoles. In a  $\beta$ -sheet, the normal modes are delocalized both along and

across  $\beta$ -strands (Figure 2A).<sup>31,34</sup> For  $\beta$ -sheets, the largest transition dipole is found at a frequency that is red-shifted from the local modes. In general, the greater the extent of delocalization, the larger the red shift. Thus, the frequency of the amide I mode of amyloid provides a measure for the size of the  $\beta$ -sheet and its rigidity (because disordered  $\beta$ -sheets have a smaller delocalization). Figure 2B shows experimental FTIR spectra of various amyloid proteins. The largest and most rigid amyloids absorb near 1620  $\text{cm}^{-1}$ , while smaller and more disordered fibers are at 1635  $\text{cm}^{-1}$ , which is typical of the bent  $\beta$ -sheets in proteins. Generally, the lower the frequency, the sharper the peak because the  $\beta$ -sheet normal mode subsumes more of the local modes.

*Isotope Labeling for Site-Specific Structural Information.* The 1620  $\text{cm}^{-1}$  normal mode of amyloids is a useful diagnostic of amyloid, but it generally cannot be assigned to a specific part of the protein without labeling of some sort. Non-natural vibrational tags can be used, such as nitriles,<sup>35</sup> but we focus here on heavy isotope labels.<sup>6,19,29,31,34,36–38</sup>

For polypeptides, one or more  $^{13}\text{C}=\text{O}^{18}\text{O}$  labels can be incorporated into a polypeptide backbone using solid-phase peptide synthesis,<sup>29,36</sup> which is a common method of synthesizing small fiber-forming peptides. Labeling with  $^{13}\text{C}=\text{O}^{18}\text{O}$  shifts the amide I band by about 64  $\text{cm}^{-1}$ .<sup>45</sup> The couplings to surrounding amide I local modes do not change, but the frequency shift decreases their effect. Thus, to a first approximation, one can consider the  $^{13}\text{C}=\text{O}^{18}\text{O}$  modes separate from the unlabeled mode. That is, the  $^{13}\text{C}=\text{O}^{18}\text{O}$  modes will form their own set of normal modes. This fact can be used to locate in-register  $\beta$ -sheets, such as those shown in Figures 1B and 3A, because isotope labeling one residue will form a column (or linear chain) of isotope-labeled residues with a red-shifted frequency. This effect has been used to study A $\beta$ , hIAPP, and other model amyloid-forming polypeptides.<sup>6,25,28,38,46–48</sup> To make sure that the red shift is indeed due to coupling and to measure the strength of that coupling, which is related to the structural disorder of the linear chain, the spectra are compared to mixtures of labeled and unlabeled peptides. Dilution of the isotope labels does not change the protein structure but breaks the delocalization (Figure 3).<sup>38</sup>

Linear chains are very good probes of parallel  $\beta$ -sheet amyloid fibers made from monomers (Figure 1C) in which each protein contributes a single  $\beta$ -strand. This approach has been used to study a series of polypeptides and model amyloid-forming peptides.<sup>6,28,38,46–49</sup> For example, by labeling a series of amino acids along the length of hIAPP, the measured couplings confirmed the ssNMR structure of hIAPP fibers.<sup>50</sup> Dunkelberger et al. showed that chemical modification of the polypeptide backbone, via deamidation of asparagine and glutamine residues, perturbs the fiber structure to abolish the coupling of in-register  $^{13}\text{C}=\text{O}^{18}\text{O}$  labels.<sup>48</sup> Additional experiments probing kinetics of these systems and others are given below. Many of our examples are from 2D IR experiments because our research group specializes in 2D IR spectroscopy. For these examples, the frequencies of the diagonal peaks in the 2D IR spectra can be interpreted in the same way as the FTIR peaks. In the last section of this Perspective, we outline some additional capabilities of 2D IR spectroscopy that are particularly valuable for studying amyloids.

*Kinetic Studies for Probing Mechanisms of Amyloid Formation.* An important capability of FTIR and 2D IR spectroscopy is that spectra can be collected rapidly and continuously, so that the structures of misfolding intermediates that may play a role

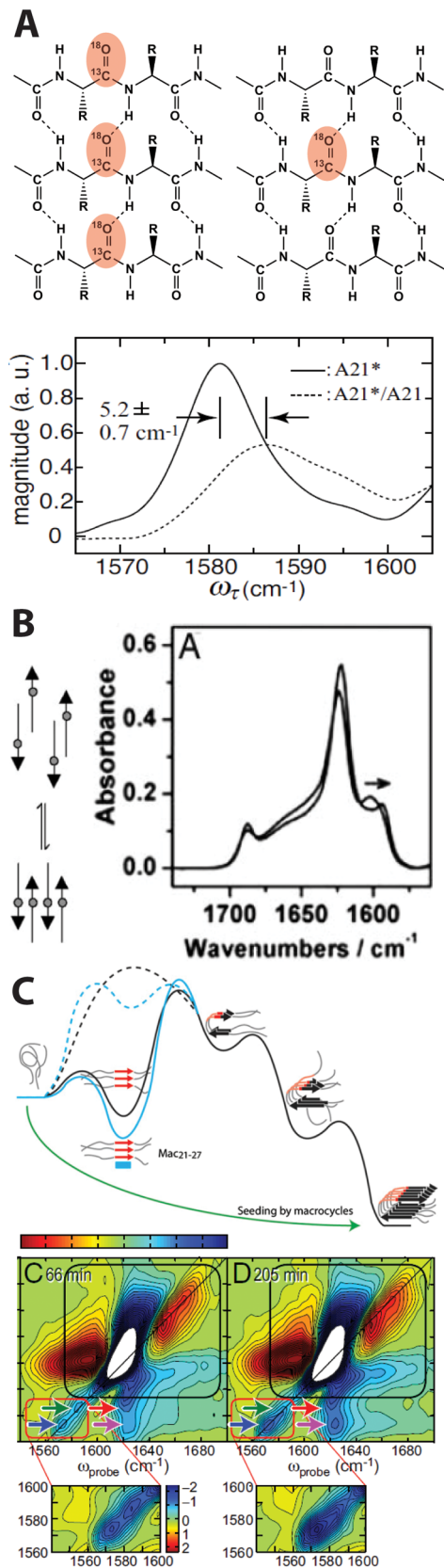


**Figure 3.** Effect of vibrational coupling in the IR spectra of  $^{13}\text{C}=^{18}\text{O}$  amyloids. (A) Parallel in-register  $\beta$ -sheets with each strand containing identical  $^{13}\text{C}=^{18}\text{O}$  labels (left, red) and dilute  $^{13}\text{C}=^{18}\text{O}$  labels (right, red). In-register labeling and isotope dilution of the amyloid peptide  $\text{A}\beta$  (bottom) demonstrated the low-frequency fully coupled labeled amide I mode and the blue shift in label frequency that occurs upon

**Figure 3. continued**

dilution with  $^{12}\text{C}=^{16}\text{O}$  residues. The lower panel is reproduced from ref 38, copyright 2008, Proceedings of the National Academy of Sciences of America. (B) Equilibration of amyloid aggregates from out-of-register to stable in-register species is accompanied by a shift in the  $^{13}\text{C}=^{18}\text{O}$  label frequency as labels (gray circles) align. Reproduced from ref 46, copyright 2005, Proceedings of the National Academy of Sciences of America. (C)  $^{13}\text{C}=^{18}\text{O}$ -labeled variants of hIAPP define the order of amino acid incorporation into amyloid  $\beta$ -sheets via a shift in label frequency and intensity and the appearance of a cross-peak between labeled and unlabeled  $\beta$ -sheets in the 2D IR spectra. A transient  $\beta$ -sheet intermediate (top panel) was identified based on the appearance of linearly coupled labels prior to stable fiber formation. Reproduced from refs 28 and 47, copyright 2013 and 2009, respectively, Proceedings of the National Academy of Sciences of America.

Isotopic dilution provides an infrared spectrum for a  $^{13}\text{C}$  monomer held in the fiber conformation.

in fiber formation or their toxicity to cells can be examined. Numerous recent studies have exploited this advantage to study the mechanisms of amyloid aggregation. Petty and Decatur used isotope-edited FTIR spectroscopy to follow the nucleation of prion peptide H1 ( $\text{PrP}_{109-122}$ ) and the rearrangement of peptides from a nonequilibrium state with out-of-register  $\beta$ -strands to an in-register equilibrium state (Figure 3B).<sup>46</sup> Shim and co-workers used 2D IR spectroscopy to follow the formation of in-register chains of  $^{13}\text{C}=^{18}\text{O}$  labels at six positions within hIAPP to determine the order of incorporation of residues into the stable fiber  $\beta$ -sheets (Figure 3C).<sup>47</sup> Additionally, the mechanisms of fibrillation inhibitors have been examined using IR spectroscopy based on their influence on the kinetics of fibrillation as well as intermediate and stable fiber structures. Middleton et al. showed that the non-amyloidogenic rat IAPP peptide interacts with hIAPP, inhibiting its aggregation while being incorporated into the fibrils that form, albeit at a slower rate.<sup>25</sup> More recently, Buchanan et al. used designed macrocyclic  $\beta$ -sheet inhibitors containing hIAPP sequences to identify an early  $\beta$ -sheet intermediate on the fibril formation pathway, by monitoring the frequency and line shape of a label in the turn region, which forms a transient extended  $\beta$ -sheet early in the aggregation process (Figure 3C).<sup>28</sup> Experiments such as these provide an important window into the misfolding processes that allow amyloidogenic proteins to transit from their native and/or denatured states to the stable amyloid well in the folding free-energy landscape (Figure 1A).

*Mixing Uniformly Labeled Proteins to Identify Structural Motifs.* The single-labeling approach for identifying parallel  $\beta$ -sheets has proven to be very useful in small polypeptide systems that can be synthesized. Single  $^{13}\text{C}=^{18}\text{O}$  labels can be incorporated into larger proteins using stop-codon replacement approaches or native chemical ligation (discussed below), but it is not clear if the parallel, in-register  $\beta$ -sheet motifs of  $\text{A}\beta$ , hIAPP, and model peptides are retained in amyloid fibers of other amyloid peptides and larger amyloid proteins. In many of the possible amyloid structures of larger proteins (Figure 1), delocalization

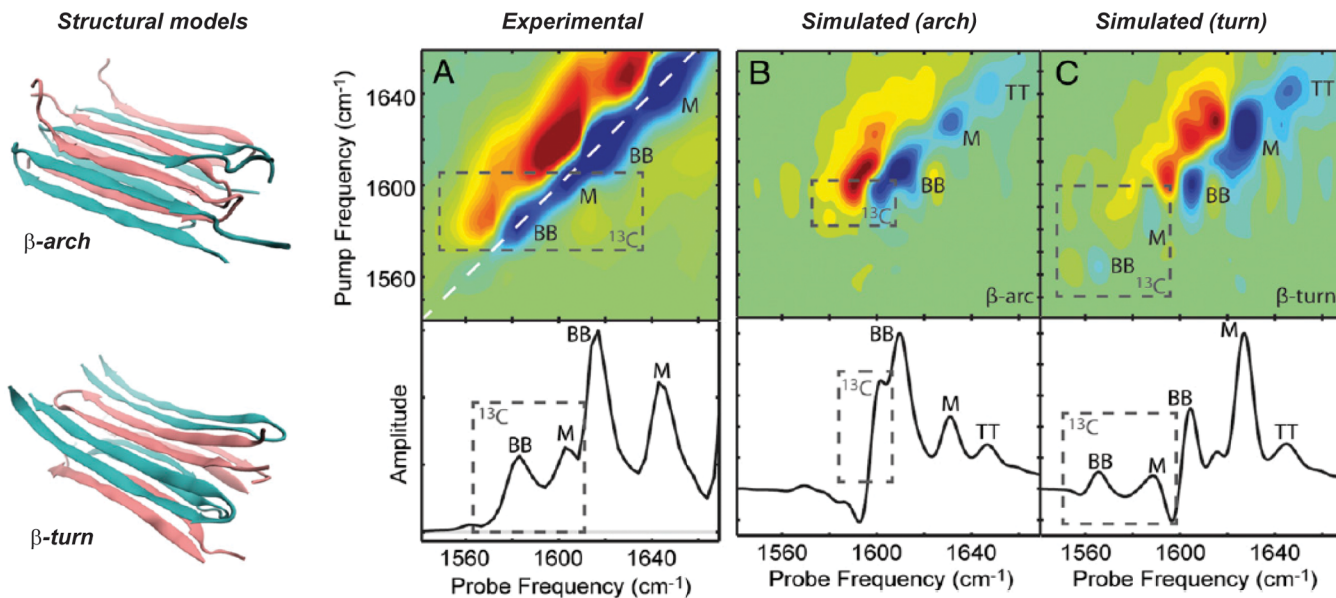


**Figure 4.** Discerning the  $\beta$ -sheet architecture of polyQ using uniform  $^{13}\text{C}$  labeling. (Left) Structural models of polyQ fiber segments in  $\beta$ -arch and  $\beta$ -turn configurations from molecular dynamics simulations. (Right) Experimental and simulated spectra of fibers and fiber models. (A) Experimental 2D IR spectrum (top) and diagonal slice (bottom) of 10%  $^{13}\text{C}$  polyQ in 90%  $^{12}\text{C}$  polyQ. Peaks arising primarily from  $^{13}\text{C}$  backbone (BB) and side-chain (M) modes are indicated in the dashed box. (B) Simulated 2D IR spectrum and diagonal slice of the  $\beta$ -arch model. (C) Simulated 2D IR spectrum and diagonal slice of the  $\beta$ -turn model. Images are reproduced from ref 37, copyright 2014, Proceedings of the National Academy of Sciences of America.

of labeled modes may not occur, and therefore, no characteristic red-shifted frequencies would be observed.

For larger proteins or amyloid motifs that have more than one  $\beta$ -strand per protein, we have instead used uniform isotope labeling, such as in our study on the tertiary structure of polyglutamine peptides in amyloid aggregates.<sup>37</sup> The structures of the polyglutamine regions in the fiber state are a longstanding problem in Huntington's disease research,<sup>51,52</sup> and a variety of competing structures have been proposed from NMR and other experiments.<sup>26,37,53</sup> Two such structures are the  $\beta$ -arch and  $\beta$ -turn models, shown in Figure 4, each of which contains polyglutamine molecules adopting two  $\beta$ -strands separated by a short turn.<sup>37</sup> The  $\beta$ -arch model contains only intermolecular hydrogen bonds and contributes only one  $\beta$ -strand per  $\beta$ -sheet, whereas in the  $\beta$ -turn model, both strands occur in the same  $\beta$ -sheet. In both structures, the side chains are intercalated to stabilize the stacked sheets. Without isotope labeling, the infrared spectra for these two models would be identical because the vibrational modes would delocalize along the  $\beta$ -sheets regardless of whether each peptide was contributing one or two  $\beta$ -strands.

To identify whether our model polyglutamine peptide, KKQ<sub>24</sub>KKW, adopted the  $\beta$ -turn,  $\beta$ -arch, or some other type of structure, we expressed the proteins and used isotope dilution. The proteins were expressed in *E. coli* so that they could be either uniformly  $^{13}\text{C}$ -labeled or left at natural abundance  $^{12}\text{C}$  (98.9%).  $^{13}\text{C}$  produces a  $39\text{ cm}^{-1}$  frequency shift of the amide I band. We formed fibers using 10%  $^{13}\text{C}$ -labeled peptides and 90% natural abundance ( $^{12}\text{C}$ ). As discussed above, the  $^{13}\text{C}$ -labeled amino acids will form normal modes separate from the  $^{12}\text{C}$  modes. At 10% dilution, there is a very small chance that any two  $^{13}\text{C}$ -labeled peptides will be hydrogen-bonded to one another in the fiber structure. As a result, the normal modes of the  $^{13}\text{C}$  region will only span that of a single protein. In essence, isotopic dilution provides an

infrared spectrum for a  $^{13}\text{C}$  monomer held in the fiber conformation (Figure 4).

We exploit the fact that the "monomer" spectra for the  $\beta$ -arch and  $\beta$ -turn models are very different from one another. The  $\beta$ -arch monomer has vibrational couplings along and between its strands, which are on opposite  $\beta$ -sheets. The distance between stacked  $\beta$ -sheets is large enough that couplings from one sheet to another can be neglected.<sup>31</sup> Thus, the monomer spectrum of the  $\beta$ -arch model is primarily that of a single  $\beta$ -strand (plus some "random coil" features caused by the loop). In contrast, the  $\beta$ -turn model has both  $\beta$ -strands in the same sheet, which are very strongly coupled. Thus, its monomer spectrum will be that of a two-stranded  $\beta$ -sheet, which has very large couplings and a large frequency shift. Thus, distinguishing one from the other by isotope dilution is quite straightforward. The experimental spectra clearly identified the  $\beta$ -turn model as the structure for this polypeptide. Computed infrared spectra from molecular dynamics simulations of the structures confirmed the conclusion.

We have also used this approach to estimate the number of  $\beta$ -strands in amyloid fibers for which there is no structural model, which has produced models such as that of  $\gamma\text{D}$ -crystallin shown in Figure 1E.<sup>19</sup> It is very simple to make uniformly labeled proteins using bacterial expression, suggesting that this approach will be a powerful way to examine many other amyloid protein structures. In addition to amyloid fibers, structural information on many protein complexes could be obtained using similar mixed-isotope studies.

*Probing the Structures of Domains Using Expressed Protein Ligation.* To obtain structural information about domains or regions of structure within a larger protein, we have adopted segmental labeling techniques. Originally utilized in NMR spectroscopy,<sup>54,55</sup> we have used expressed protein ligation to produce  $^{13}\text{C}$ -labeled continuous spans of sequence within the

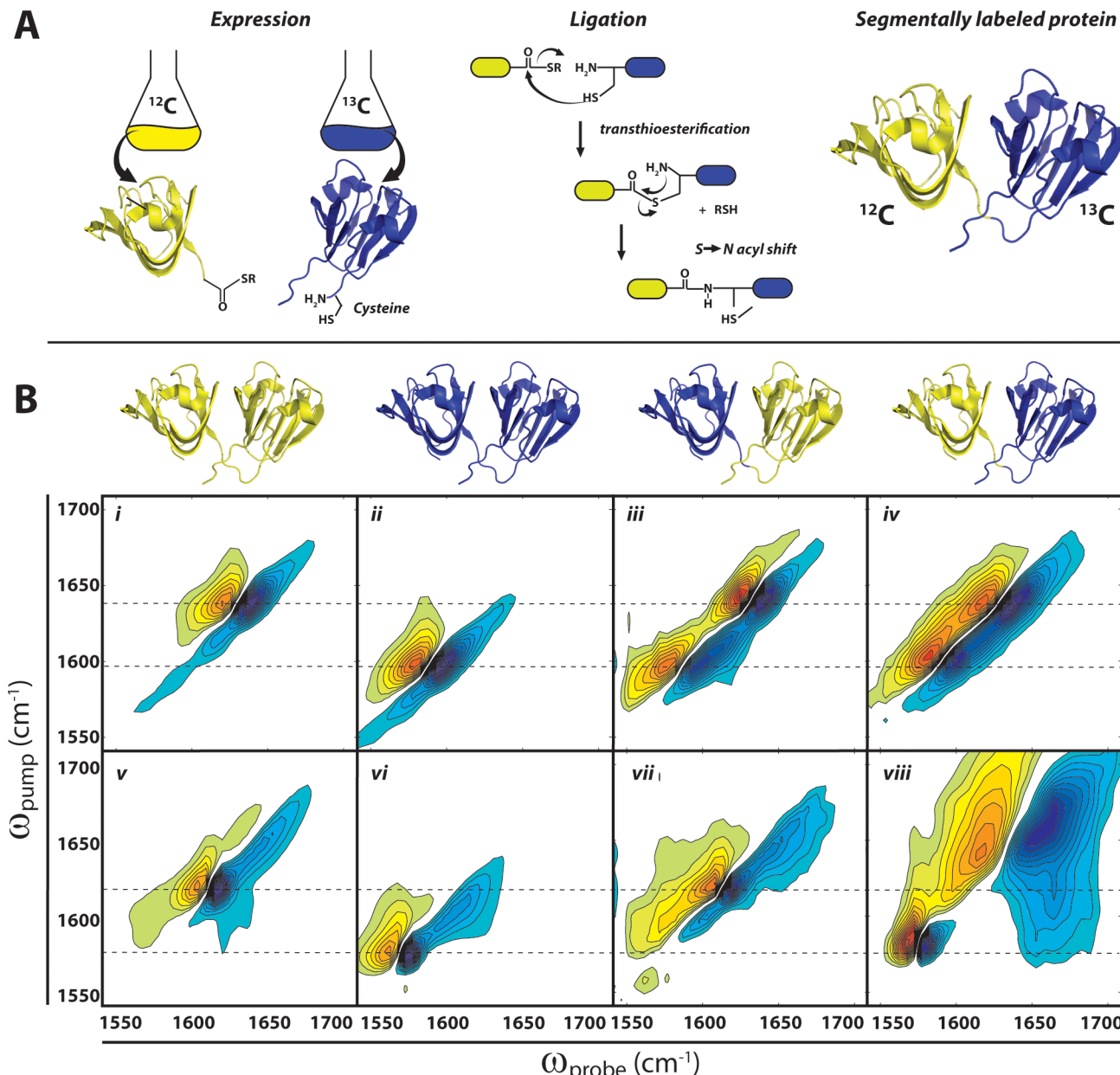


**Figure 5.** Segmental <sup>13</sup>C labeling of  $\gamma$ D-crystallin. (A) Use of expressed protein ligation to generate segmentally labeled proteins. Individual domains are expressed separately in *E. coli* with reactive termini (C-terminal thioester and N-terminal cysteine), and subsequent transthiioesterification and peptide bond formation via an S → N acyl shift generates the full-length protein with one isotope-labeled domain. (B) 2D IR spectra of  $\gamma$ D-crystallin. (Top row) Native structures showing the location of <sup>12</sup>C (yellow) and <sup>13</sup>C (blue) domains in unlabeled (<sup>12</sup>C), uniformly <sup>13</sup>C-labeled, C-terminally labeled, and N-terminally <sup>13</sup>C-labeled  $\gamma$ D-crystallin. (Middle row) (i–iv) 2D IR spectra of native  $\gamma$ D-crystallin labeling variants. (Bottom row) (v–viii) 2D IR spectra of acid-induced amyloid fibers of  $\gamma$ D-crystallin labeling variants. All 2D IR spectra are plotted based on data first reported in ref 19. Dashed lines indicate  $\omega_{\text{pump}}$  for labeled and unlabeled native  $\beta$ -sheets (i–iv) and amyloid  $\beta$ -sheets (v–viii).

protein.<sup>19,21,30,56</sup> This biochemical method, shown schematically in Figure 5A, is a way of semisynthesizing proteins. One expresses the protein in pieces so that one or the other piece can be uniformly <sup>13</sup>C-labeled.<sup>57</sup> The pieces are then ligated under very mild mixing conditions. Expressed protein ligation is particularly well-suited for selectively labeling domains of proteins because individual domains often express well, and their association can aid the ligation. Isotope labeling domains is an important new way of studying proteins, including amyloid aggregates, with infrared spectroscopy.

Using segmental <sup>13</sup>C labeling, we discovered some surprising facts about  $\gamma$ D-crystallin. A common property of many amyloid

Isotope labeling domains is an important new way of studying proteins, including amyloid aggregates, with infrared spectroscopy.

fiber-forming proteins is the existence of repeated sequence motifs that favor self-association of proteins into ordered aggregates, often with multiple  $\beta$ -strands forming one or more  $\beta$ -sheets (Figure 1C,E). These repeats may be short such as in

the 6–9 residue repeats of prion proteins or may span entire domains of proteins such as in the  $\beta\gamma$ -crystallins.<sup>19,21</sup> Additionally, such proteins typically contain nonrepeat sequence regions. The ability of individual amyloidogenic repeat sequence segments to form fibers in isolation has been well-established in many systems, including prion fragments that have been characterized in detail by X-ray crystallography.<sup>11</sup> A key structural question in such systems is which regions of sequence form the amyloid  $\beta$ -sheets and which regions lie outside of the stable  $\beta$ -sheet amyloid core. This question is particularly relevant for  $\gamma$ D-crystallin, which is a 173 amino acid eye lens protein.  $\gamma$ D-Crystallin has two domains with nearly identical three-dimensional structures in the native state.<sup>58</sup> At low pH, the full-length protein as well as each of its individual domains can form amyloid fibers, as shown in electron microscopy, dye binding, and FTIR experiments.<sup>43</sup> The domains are so similar that one might expect either or both of the domains to contribute to the amyloid fibers, but these experiments do not distinguish one domain from the other. To address this question, we labeled the two domains with  $^{13}\text{C}$  individually, using expressed protein ligation to reconstitute segmentally labeled full-length proteins.<sup>19</sup>  $^{13}\text{C}$  labeling produces a  $40 \text{ cm}^{-1}$  red shift in the amide I signal; therefore, a  $^{13}\text{C}$ -labeled domain can be resolved from an unlabeled domain in either FTIR or 2D IR spectra. Upon acid-induced aggregation, it was obvious that only the C-terminal domain forms amyloid  $\beta$ -sheets, while the entire N-terminal domain becomes extremely disordered. This result, discussed in detail in ref 19, was very surprising considering the aforementioned fragment studies<sup>43</sup> that pointed to the N-terminal domain as the source of amyloid  $\beta$ -sheets. Using enzymatic digestion and mass spectrometric sequencing of residual  $\beta$ -sheet regions, we confirmed the conclusions from 2D IR spectroscopy.<sup>21</sup> Subsequently, we applied these methods to other aggregates of  $\gamma$ D-crystallin formed by UV-B radiation<sup>30</sup> and thermal denaturation<sup>56</sup> and showed that while the C-terminal domain dominates the amyloid  $\beta$ -sheets in each case, alternative  $\beta$ -sheet structures can be formed that contain different sequence compositions as well as covalent modifications to the polypeptide chain. These results demonstrated not only that segmental labeling is useful in IR studies of large amyloid proteins but also that the amyloid state itself is diverse and can accommodate a broad range of structural configurations.

*Additional Information Content of 2D IR Spectroscopy.* The strategies listed above for studying amyloid structures can be performed with either FTIR or 2D IR spectroscopy because only the frequencies are needed for structural information. That being said, 2D IR spectroscopy provides many more observables for protein structure than are available from FTIR spectroscopy, such as the anharmonic shift, 2D line shapes, lifetimes, and vibrational dynamics<sup>59,60</sup> all of which are sensitive measures of protein secondary structure. The theory and implementation of 2D IR spectroscopy are described in detail elsewhere.<sup>34</sup> Here, we focus on a single aspect that turns out to be enormously beneficial: the nonlinearity of the signal strength. An FTIR signal scales linearly with the concentration of the molecular species ( $c$ ) and the absorptivity ( $\epsilon$ ), for example,  $ce$ . A 2D IR spectrum scales linearly with the concentration and quadratically with the absorptivity, for example,  $ce^2$  (one  $\epsilon$  for each axis of the spectrum). As a result, if two samples have the same optical density because one was more concentrated while the other had a larger absorptivity, then the FTIR signal would be the same for both, but the 2D

IR signal would be larger for the sample with the larger absorptivity. As a result, the peaks in 2D IR spectra are sharper, and baselines caused by weak absorbers are effectively eliminated. Moreover, this fact can be used to identify secondary structures<sup>61</sup> because the absorptivity scales with the delocalization of the normal modes. For example, the amyloid mode that is characteristic of  $\beta$ -sheets can involve as many as 12 oscillators, which means that its absorptivity is 12 times larger than that for a single amino acid. This fact means that 2D IR spectroscopy is much more sensitive to secondary structures than is FTIR spectroscopy. Thus, by measuring the absorptivity, secondary structure assignments can be much more rigorous, whether or not isotope labels are used. A terrific application is distinguishing between  $\alpha$ -helices and random coils. These two secondary structures have very similar frequencies, which makes their assignment from FTIR spectroscopy tentative. However, the transition dipole of  $\alpha$ -helices is much larger than random coils because five amino acids contribute to the A mode of  $\alpha$ -helices, whereas random structures have very little delocalization. As a result, the 2D IR spectrum of an  $\alpha$ -helix is much more prominent than that of a random coil (in addition to having a narrower line width and a smaller anharmonic shift).<sup>62</sup>

2D IR spectroscopy provides many more observables for protein structure than are available from FTIR spectroscopy.

*Outlook.* The infrared techniques described in this Perspective hold a great deal of promise for studying amyloid architectures and aggregation mechanisms. The main challenges to utilizing these methods are the production of the labeled molecules and the interpretation of congested infrared spectra. Peptide synthesis and protein expression are routine, and therefore, most of the labeling techniques above are straightforward. More advanced labeling methods are yet to be used, such as incorporation of site-specific isotope labels or non-natural vibrational chromophores in large proteins using stop-codon replacement<sup>63,64</sup> or cell-free expression.<sup>65</sup> Side chains could also be labeled.<sup>35</sup> Interpretation of the infrared spectra can be done qualitatively, but incredible advances have also occurred in the past few years for calculating infrared spectra from molecular dynamics simulations. Spectra can now be calculated with an accuracy of a few wavenumbers,<sup>45</sup> enabling hypothesized structures to be tested against experiment. 2D IR spectrometers are now commercially available, making this technology available to a wider range of scientists.<sup>66</sup> Isotope labeling approaches are not relegated solely to amyloid proteins, so the techniques described here could also be applied to studies in protein folding,<sup>67</sup> drug binding, membrane protein dynamics, and a variety of other areas. Infrared spectroscopy has a long history in biophysics.<sup>68,69</sup> The combination of new labeling methods, 2D IR spectroscopy, and quantitative simulations are bringing about its renaissance in structural biology.

## ■ AUTHOR INFORMATION

### Corresponding Author

\*E-mail: zanni@chem.wisc.edu.

**Notes**

The authors declare the following competing financial interest(s): Martin T. Zanni is co-owner of PhaseTech Spectroscopy, Inc., which manufactures 2D IR spectrometers.

**Biographies**

**Sean D. Moran** completed his Ph.D in bioinorganic/biophysical chemistry at Columbia University (2008) with Brian R. Gibney and studied protein aggregation in Martin Zanni's lab at the University of Wisconsin—Madison (2009–2013). He will be joining the Department of Chemistry and Biochemistry at SIU—Carbondale as an Assistant Professor in 2014.

**Martin T. Zanni** is the Meloche—Bascom Professor of Chemistry at the University of Wisconsin—Madison. He specializes in multidimensional spectroscopies, like 2D-infrared and 2D-whitelight spectroscopy, and their application to topics in biophysics, biochemistry, and the energy sciences.

**ACKNOWLEDGMENTS**

This work was supported by NIH NIDDK Grant DK79895.

**REFERENCES**

- (1) Chiti, F.; Dobson, C. M. Protein Misfolding, Functional Amyloid, and Human Disease. *Annu. Rev. Biochem.* **2006**, *75*, 333–366.
- (2) Eisenberg, D.; Jucker, M. The Amyloid State of Proteins in Human Diseases. *Cell* **2012**, *148*, 1188–1203.
- (3) Fowler, D. M.; Koulov, A. V.; Balch, W. E.; Kelly, J. W. Functional Amyloid—from Bacteria to Humans. *Trends Biochem. Sci.* **2007**, *32*, 217–224.
- (4) Hanczyc, P.; Samoc, M.; Norden, B. Multiphoton Absorption in Amyloid Protein Fibres. *Nat. Photonics* **2013**, *7*, 969–972.
- (5) del Mercato, L. L.; Pompa, P. P.; Maruccio, G.; Torre, A. D.; Sabella, S.; Tamburro, A. M.; Cingolani, R.; Rinaldi, R. Charge Transport and Intrinsic Fluorescence in Amyloid-Like Fibrils. *Proc. Natl. Acad. Sci. U.S.A.* **2007**, *104*, 18019–18024.
- (6) Rodriguez-Perez, J. C.; Hamley, I. W.; Gras, S. L.; Squires, A. M. Local Orientational Disorder in Peptide Fibrils Probed by a Combination of Residue-Specific  $^{13}\text{C}$ – $^{18}\text{O}$  Labelling, Polarised Infrared Spectroscopy and Molecular Combing. *Chem. Commun.* **2012**, *48*, 11835–11837.
- (7) Goldschmidt, L.; Teng, P. K.; Riek, R.; Eisenberg, D. Identifying the Amylome, Proteins Capable of Forming Amyloid-Like Fibrils. *Proc. Natl. Acad. Sci. U.S.A.* **2010**, *107*, 3487–3492.
- (8) Hane, F. Are Amyloid Fibrils Molecular Spandrels? *FEBS Lett.* **2013**, *587*, 3617–3619.
- (9) Jahn, T. R.; Makin, O. S.; Morris, K. L.; Marshall, K. E.; Tian, P.; Sikorski, P.; Serpell, L. C. The Common Architecture of Cross- $\beta$  Amyloid. *J. Mol. Biol.* **2010**, *395*, 717–727.
- (10) Kurouski, D.; Deckert-Gaudig, T.; Deckert, V.; Lednev, I. K. Structure and Composition of Insulin Fibril Surfaces Probed by TERS. *J. Am. Chem. Soc.* **2012**, *134*, 13323–13329.
- (11) Nelson, R.; Sawaya, M. R.; Balbirnie, M.; Madsen, A. O.; Riek, C.; Grothe, R.; Eisenberg, D. Structure of the Cross-Beta Spine of Amyloid-Like Fibrils. *Nature* **2005**, *435*, 773–778.
- (12) Luca, S.; Yau, W.-M.; Leapman, R.; Tycko, R. Peptide Conformation and Supramolecular Organization in Amylin Fibrils: Constraints from Solid-State NMR. *Biochemistry* **2007**, *46*, 13505–13522.
- (13) Petkova, A. T.; Yau, W.-M.; Tycko, R. Experimental Constraints on Quaternary Structure in Alzheimer's  $\beta$ -Amyloid Fibrils. *Biochemistry* **2005**, *45*, 498–512.
- (14) Qiang, W.; Yau, W.-M.; Luo, Y.; Mattson, M. P.; Tycko, R. Antiparallel  $\beta$ -Sheet Architecture in Iowa-Mutant  $\beta$ -Amyloid Fibrils. *Proc. Natl. Acad. Sci. U.S.A.* **2012**, *109*, 4443–4448.
- (15) Tycko, R. Molecular Structure of Amyloid Fibrils: Insights from Solid-State NMR. *Q. Rev. Biophys.* **2006**, *39*, 1–55.
- (16) Bertini, I.; Gonnelli, L.; Luchinat, C.; Mao, J.; Nesi, A. A New Structural Model of  $\text{A}\beta_{40}$  Fibrils. *J. Am. Chem. Soc.* **2011**, *133*, 16013–16022.
- (17) Wasmer, C.; Lange, A.; Van Melckebeke, H.; Siemer, A. B.; Riek, R.; Meier, B. H. Amyloid Fibrils of the HET-s(218–289) Prion Form a  $\beta$  Solenoid with a Triangular Hydrophobic Core. *Science* **2008**, *319*, 1523–1526.
- (18) Chen, M.; Margittai, M.; Chen, J.; Langen, R. Investigation of  $\alpha$ -Synuclein Fibril Structure by Site-Directed Spin Labeling. *J. Biol. Chem.* **2007**, *282*, 24970–24979.
- (19) Moran, S. D.; Woys, A. M.; Buchanan, L. E.; Bixby, E.; Decatur, S. M.; Zanni, M. T. Two-Dimensional IR Spectroscopy and Segmental  $^{13}\text{C}$  Labeling Reveals the Domain Structure of Human gamma D-Crystallin Amyloid Fibrils. *Proc. Natl. Acad. Sci. U.S.A.* **2012**, *109*, 3329–3334.
- (20) Tsutsumi, M.; Otaki, J. M. Parallel and Antiparallel  $\beta$ -Strands Differ in Amino Acid Composition and Availability of Short Constituent Sequences. *J. Chem. Inf. Model.* **2011**, *51*, 1457–1464.
- (21) Moran, S. D.; Decatur, S. M.; Zanni, M. T. Structural and Sequence Analysis of the Human  $\gamma$ D-Crystallin Amyloid Fibril Core Using 2D IR Spectroscopy, Segmental  $^{13}\text{C}$  Labeling, and Mass Spectrometry. *J. Am. Chem. Soc.* **2012**, *134*, 18410–18416.
- (22) Liu, Y.; Eisenberg, D. 3D Domain Swapping: As Domains Continue to Swap. *Protein Sci.* **2002**, *11*, 1285–1299.
- (23) Teoh, C. L.; Pham, C. L. L.; Todorova, N.; Hung, A.; Lincoln, C. N.; Lees, E.; Lam, Y. H.; Binger, K. J.; Thomson, N. H.; Radford, S. E.; et al. A Structural Model for Apolipoprotein C-II Amyloid Fibrils: Experimental Characterization and Molecular Dynamics Simulations. *J. Mol. Biol.* **2011**, *405*, 1246–1266.
- (24) Hartl, F. U.; Bracher, A.; Hayer-Hartl, M. Molecular Chaperones in Protein Folding and Proteostasis. *Nature* **2011**, *475*, 324–332.
- (25) Middleton, C. T.; Marek, P.; Cao, P.; Chiu, C. C.; Singh, S.; Woys, A. M.; de Pablo, J. J.; Raleigh, D. P.; Zanni, M. T. Two-Dimensional Infrared Spectroscopy Reveals the Complex Behaviour of an Amyloid Fibril Inhibitor. *Nature Chem.* **2012**, *4*, 355–360.
- (26) Kajava, A. V.; Baxa, U.; Steven, A. C. Beta Arcades: Recurring Motifs in Naturally Occurring and Disease-Related Amyloid Fibrils. *FASEB J.* **2010**, *24*, 1311–1319.
- (27) Janowski, R.; Kozak, M.; Abrahamson, M.; Grubb, A.; Jaskolski, M. 3D Domain-Swapped Human Cystatin C with Amyloidlike Intermolecular  $\beta$ -Sheets. *Proteins* **2005**, *61*, 570–578.
- (28) Buchanan, L. E.; Dunkelberger, E. B.; Tran, H. Q.; Cheng, P. N.; Chiu, C. C.; Cao, P.; Raleigh, D. P.; de Pablo, J. J.; Nowick, J. S.; Zanni, M. T. Mechanism of IAPP Amyloid Fibril Formation Involves an Intermediate with a Transient  $\beta$ -Sheet. *Proc. Natl. Acad. Sci. U.S.A.* **2013**, *110*, 19285–19290.
- (29) Middleton, C. T.; Woys, A. M.; Mukherjee, S. S.; Zanni, M. T. Residue-Specific Structural Kinetics of Proteins Through the Union of Isotope Labeling, Mid-IR Pulse Shaping, and Coherent 2D IR Spectroscopy. *Methods* **2010**, *52*, 12–22.
- (30) Moran, S. D.; Zhang, T. O.; Decatur, S. M.; Zanni, M. T. Amyloid Fiber Formation in Human  $\gamma$ D-Crystallin Induced by UV-B Photodamage. *Biochemistry* **2013**, *52*, 6169–6181.
- (31) Strasfeld, D. B.; Ling, Y. L.; Gupta, R.; Raleigh, D. P.; Zanni, M. T. Strategies for Extracting Structural Information from 2D IR Spectroscopy of Amyloid: Application to Islet Amyloid Polypeptide. *J. Phys. Chem. B* **2009**, *113*, 15679–15691.
- (32) Londergan, C. H.; Wang, J.; Axelsen, P. H.; Hochstrasser, R. M. Two-Dimensional Infrared Spectroscopy Displays Signatures of Structural Ordering in Peptide Aggregates. *Biophys. J.* **2006**, *90*, 4672–4685.
- (33) Hahn, S.; Kim, S. S.; Lee, C.; Cho, M. Characteristic Two-Dimensional IR Spectroscopic Features of Antiparallel and Parallel  $\beta$ -Sheet Polypeptides: Simulation Studies. *J. Chem. Phys.* **2005**, *123*, 084905.
- (34) Hamm, P.; Zanni, M. *Concepts and Methods of 2D Infrared Spectroscopy*; Cambridge University Press: New York, 2011.
- (35) Kim, H.; Cho, M. Infrared Probes for Studying the Structure and Dynamics of Biomolecules. *Chem. Rev.* **2013**, *113*, 5817–5847.

- (36) Arkin, I. T. Isotope-Edited IR Spectroscopy for the Study of Membrane Proteins. *Curr. Opin. Chem. Biol.* **2006**, *10*, 394–401.
- (37) Buchanan, L. E.; Carr, J. K.; Fluit, A. M.; Hoganson, A. J.; Moran, S. D.; de Pablo, J. J.; Skinner, J. L.; Zanni, M. T. Structural Motif of Polyglutamine Amyloid Fibrils Discerned with Mixed-Isotope Infrared Spectroscopy. *Proc. Natl. Acad. Sci. U.S.A.* **2014**, *111*, 5796–5801.
- (38) Kim, Y. S.; Liu, L.; Axelsen, P. H.; Hochstrasser, R. M. Two-Dimensional Infrared Spectra of Isotopically Diluted Amyloid Fibrils from  $\text{A}\beta 40$ . *Proc. Natl. Acad. Sci. U.S.A.* **2008**, *105*, 7720–7725.
- (39) Hiramatsu, H.; Kitagawa, T. FT-IR Approaches on Amyloid Fibril Structure. *Biochim. Biophys. Acta* **2005**, *1753*, 100–107.
- (40) Sarroukh, R.; Goormaghtigh, E.; Ruyschaert, J.-M.; Raussens, V. ATR-FTIR: A “Rejuvenated” Tool to Investigate Amyloid Proteins. *Biochim. Biophys. Acta, Biomembr.* **2013**, *1828*, 2328–2338.
- (41) Shim, S.-H.; Strasfeld, D. B.; Ling, Y. L.; Zanni, M. T. Automated 2D IR Spectroscopy Using a Mid-IR Pulse sShaper and Application of This Technology to the Human Islet Amyloid Polypeptide. *Proc. Natl. Acad. Sci. U.S.A.* **2007**, *104*, 14197–14202.
- (42) Ostapchenko, V. G.; Sawaya, M. R.; Makarava, N.; Savtchenko, R.; Nilsson, K. P. R.; Eisenberg, D.; Baskakov, I. V. Two Amyloid States of the Prion Protein Display Significantly Different Folding Patterns. *J. Mol. Biol.* **2010**, *400*, 908–921.
- (43) Papanikolopoulou, K.; Mills-Henry, I.; Tho, S. L.; Wang, Y. T.; Gross, A. A. R.; Kirschner, D. A.; Decatur, S. M.; King, J. Formation of Amyloid Fibrils in vitro by Human  $\gamma\text{D}$ -Crystallin and Its Isolated Domains. *Mol. Vis.* **2008**, *14*, 81–89.
- (44) Conway, K. A.; Harper, J. D.; Lansbury, P. T. Fibrils Formed In Vitro from  $\alpha$ -Synuclein and Two Mutant Forms Linked to Parkinson’s Disease are Typical Amyloid. *Biochemistry* **2000**, *39*, 2552–2563.
- (45) Woys, A. M.; Almeida, A. M.; Wang, L.; Chiu, C.-C.; McGovern, M.; de Pablo, J. J.; Skinner, J. L.; Gellman, S. H.; Zanni, M. T. Parallel  $\beta$ -Sheet Vibrational Couplings Revealed by 2D IR Spectroscopy of an Isotopically Labeled Macrocycle: Quantitative Benchmark for the Interpretation of Amyloid and Protein Infrared Spectra. *J. Am. Chem. Soc.* **2012**, *134*, 19118–19128.
- (46) Petty, S. A.; Decatur, S. M. Intersheet Rearrangement of Polypeptides during Nucleation of  $\beta$ -sheet Aggregates. *Proc. Natl. Acad. Sci. U.S.A.* **2005**, *102*, 14272–14277.
- (47) Shim, S.-H.; Gupta, R.; Ling, Y. L.; Strasfeld, D. B.; Raleigh, D. P.; Zanni, M. T. Two-Dimensional IR Spectroscopy and Isotope Labeling Defines the Pathway of Amyloid Formation with Residue-Specific Resolution. *Proc. Natl. Acad. Sci. U.S.A.* **2009**, *106*, 6614–6619.
- (48) Dunkelberger, E. B.; Buchanan, L. E.; Marek, P.; Cao, P.; Raleigh, D. P.; Zanni, M. T. Deamidation Accelerates Amyloid Formation and Alters Amylin Fiber Structure. *J. Am. Chem. Soc.* **2012**, *134*, 12658–12667.
- (49) Chi, H.; Welch, W. R. W.; Kubelka, J.; Keiderling, T. A. Insight into the Packing Pattern of  $\beta 2$  Fibrils: A Model Study of Glutamic Acid Rich Oligomers with  $^{13}\text{C}$  Isotopic Edited Vibrational Spectroscopy. *Biomacromolecules* **2013**, *14*, 3880–3891.
- (50) Wang, L.; Middleton, C. T.; Singh, S.; Reddy, A. S.; Woys, A. M.; Strasfeld, D. B.; Marek, P.; Raleigh, D. P.; de Pablo, J. J.; Zanni, M. T.; Skinner, J. L. 2D IR Spectroscopy of Human Amylin Fibrils Reflects Stable  $\beta$ -Sheet Structure. *J. Am. Chem. Soc.* **2011**, *133*, 16062–16071.
- (51) Lee, W.-C. M.; Yoshihara, M.; Littleton, J. T. Cytoplasmic Aggregates Trap Polyglutamine-Containing Proteins and Block Axonal Transport in a Drosophila Model of Huntington’s Disease. *Proc. Natl. Acad. Sci. U.S.A.* **2004**, *101*, 3224–3229.
- (52) Heck, B. S.; Doll, F.; Hauser, K. Length-Dependent Conformational Transitions of Polyglutamine Repeats as Molecular Origin of Fibril Initiation. *Biophys. Chem.* **2014**, *185*, 47–57.
- (53) Kar, K.; Hoop, C. L.; Drombosky, K. W.; Baker, M. A.; Kodali, R.; Arduini, I.; van der Wel, P. C.; Horne, W. S.; Wetzel, R.  $\beta$ -Hairpin-Mediated Nucleation of Polyglutamine Amyloid Formation. *J. Mol. Biol.* **2013**, *425*, 1183–1197.
- (54) Ohki, S.-y.; Kainosh, M. Stable Isotope Labeling Methods for Protein NMR Spectroscopy. *Prog. Nucl. Magn. Reson. Spectrosc.* **2008**, *53*, 208–226.
- (55) Skrisovska, L.; Schubert, M.; Allain, F. d. r. Recent Advances in Segmental Isotope Labeling of Proteins: NMR Applications to Large Proteins and Glycoproteins. *J. Biomol. NMR* **2010**, *46*, 51–65.
- (56) Moran, S. D.; Zhang, T. O.; Zanni, M. T. An Alternative Structural Isoform in Amyloid-Like Aggregates Formed from Thermally Denatured Human  $\gamma\text{D}$ -Crystallin. *Protein Sci.* **2014**, *23*, 321–331.
- (57) Flavell, R. R.; Muir, T. W. Expressed Protein Ligation (EPL) in the Study of Signal Transduction, Ion Conduction, and Chromatin Biology. *Acc. Chem. Res.* **2008**, *42*, 107–116.
- (58) Basak, A.; Bateman, O.; Slingsby, C.; Pande, A.; Asherie, N.; Ogun, O.; Benedek, G. B.; Pande, J. High-Resolution X-ray Crystal Structures of Human  $\gamma\text{D}$  Crystallin (1.25 Å) and the R58H Mutant (1.15 Å) Associated with Aculeiform Cataract. *J. Mol. Biol.* **2003**, *328*, 1137–1147.
- (59) Middleton, C. T.; Buchanan, L. E.; Dunkelberger, E. B.; Zanni, M. T. Utilizing Lifetimes to Suppress Random Coil Features in 2D IR Spectra of Peptides. *J. Phys. Chem. Lett.* **2011**, *2*, 2357–2361.
- (60) Rubtsov, I. V. Relaxation-Assisted Two-Dimensional Infrared (RA 2DIR) Method: Accessing Distances over 10 Å and Measuring Bond Connectivity Patterns. *Acc. Chem. Res.* **2009**, *42*, 1385–94.
- (61) Grechko, M.; Zanni, M. T. Quantification of Transition Dipole Strengths Using 1D and 2D Spectroscopy for the Identification of Molecular Structures via Exciton Delocalization: Application to  $\alpha$ -Helices. *J. Chem. Phys.* **2012**, *137*, 184202.
- (62) Ling, Y. L.; Strasfeld, D. B.; Shim, S.-H.; Raleigh, D. P.; Zanni, M. T. Two-Dimensional Infrared Spectroscopy Provides Evidence of an Intermediate in the Membrane-Catalyzed Assembly of Diabetic Amyloid. *J. Phys. Chem. B* **2009**, *113*, 2498–2505.
- (63) Thielges, M. C.; Axup, J. Y.; Wong, D.; Lee, H. S.; Chung, J. K.; Schultz, P. G.; Fayer, M. D. Two-Dimensional IR Spectroscopy of Protein Dynamics Using Two Vibrational Labels: A Site-Specific Genetically Encoded Unnatural Amino Acid and an Active Site Ligand. *J. Phys. Chem. B* **2011**, *115*, 11294–11304.
- (64) Wang, L.; Xie, J.; Schultz, P. G. Expanding the Genetic Code. *Annu. Rev. Biophys. Biomol. Struct.* **2006**, *35*, 225–249.
- (65) Bernhard, F.; Tozawa, Y. Cell-Free Expression—Making a Mark. *Curr. Opin. Struct. Biol.* **2013**, *23*, 374–80.
- (66) Skoff, D. R.; Laaser, J. E.; Mukherjee, S. S.; Middleton, C. T.; Zanni, M. T. Simplified and Economical 2D IR Spectrometer Design Using a Dual Acousto-Optic Modulator. *Chem. Phys.* **2013**, *422*, 8–15.
- (67) Tucker, M. J.; Abdo, M.; Courter, J. R.; Chen, J.; Brown, S. P.; Smith, A. B.; Hochstrasser, R. M. Nonequilibrium Dynamics of Helix Reorganization Observed by Transient 2D IR Spectroscopy. *Proc. Natl. Acad. Sci. U.S.A.* **2013**, *110*, 17314–17319.
- (68) DeGrip, W. J.; Gray, D.; Gillespie, J.; Bovee, P. H. M.; Berg, E. M. M. V. D.; Lugtenburg, J.; Rothschild, K. J. Photoexcitation of Rhodopsin: Conformation Changes in the Chromophore, Protein and Associated Lipids as Determined by FTIR Difference Spectroscopy. *Photochem. Photobiol.* **1988**, *48*, 497–504.
- (69) Jung, C. Insight into Protein Structure and Protein–Ligand Recognition by Fourier Transform Infrared Spectroscopy. *J. Mol. Recognit.* **2000**, *13*, 325–351.